THE UNIVERSITY *of* EDINBURGH

Edinburgh Research Explorer

The effect of Knudsen layers on rarefied cylindrical Couette gas flows

The Effect of Knudsen Layers on Rarefied Cylindrical Couette Gas Flows

Nishanth Dongari[1,2*], Robert W. Barber[2], David R. Emerson[2], Stefan K. Stefanov[3], Yonghao Zhang[1] and Jason M. Reese[1]

[1]*Department of Mechanical & Aerospace Engineering, University of Strathclyde, Glasgow G1 1XJ, UK*

[2]*Centre for Microfluidics and Microsystems Modelling, STFC Daresbury Laboratory, Warrington WA4 4AD, UK*

[3]*Institute of Mechanics, Bulgarian Academy of Sciences, Acad. G. Bonchev Str., Bl. 4, Sofia 1113, Bulgaria*

[*]*e-mail: nishanth.dongari@strath.ac.uk*

Abstract

We investigate a power-law probability distribution function to describe the mean free path of rarefied gas molecules in non-planar geometries. A new curvature-dependent model is derived by taking into account the boundary-limiting effects on the molecular mean free path for surfaces with both convex and concave curvatures. The Navier-Stokes constitutive relations and the velocity-slip boundary conditions are then modified based on this power-law scaling through the transport property expressions in terms of the mean free path. Velocity profiles for isothermal cylindrical Couette flow are obtained using this power-law model and compared with direct simulation Monte Carlo (DSMC) data. We demonstrate that our model is more accurate than the classical slip solution, and we are able to capture important non-linear trends associated with the non-equilibrium physics of the Knudsen layer. In addition, we establish a new criterion for the critical accommodation coefficient that leads to the non-intuitive phenomenon of velocity inversion. The power-law model predicts that the critical accommodation coefficient is significantly lower than that calculated using the classical slip solution, and is in good agreement with available DSMC data. Our proposed constitutive scaling for non-planar surfaces is based on simple physical arguments and can be readily implemented in conventional fluid dynamics codes for arbitrary geometric configurations of microfluidic systems.

Keywords: molecular mean free path, Knudsen layer, cylindrical Couette flow, velocity inversion, curvature effects, gas micro flows, rarefied gas dynamics

1   Introduction

In rarefied/micro gas flows, the behavior of the gas near a solid boundary is dominated by surface and near-surface interactions and leads to the formation of a Knudsen layer. This is a local thermodynamically non-equilibrium region of thickness $O(\lambda)$ from the surface, where λ is the mean free path (MFP) of the gas. In this Knudsen layer, molecular collisions are considerably modified due to the presence of the solid boundary with a corresponding reduction in the mean time between collisions, i.e. the MFP of the gas will effectively be reduced and will also vary non-linearly in this thin layer (Stops 1970). Linear constitutive relations for shear stress and heat flux are also no longer valid in the Knudsen layer (Burnett 1935, Grad 1949, Chapman and Cowling 1970).

The behavior of a rarefied gas can accurately be described by the Boltzmann equation (Cercignani 1988, Sone 2002). However, directly solving the Boltzmann equation for practical applications remains computationally challenging due to the complicated structure of the molecular collision term. The direct simulation Monte Carlo (DSMC) method (Bird 1994) provides an excellent alternative approach for solving high-speed rarefied flows. Unfortunately, the computational cost of the DSMC method for low-speed flows in the slip- and transition-flow regimes is still formidable. Many researchers developing engineering applications have instead proposed modifications to the velocity-slip boundary condition originally proposed by Maxwell (1879). This has generally led to first- and second-order treatments of the velocity gradient at the wall (see Beskok 2001, Barber and Emerson 2006), but with limited success because this approach fails to reproduce the non-linear stress/strain-rate relationship observed in the Knudsen layer.

Alternative strategies are to introduce a slip coefficient that depends on the Knudsen number (Bahukudumbi et al. 2003) or to introduce an effective viscosity term. The latter approach has met with some engineering success (Veijola et al. 1995; Bahukudumbi et al. 2003; Dongari et al. 2009) but has relied on fitting data to solutions from the Boltzmann equation. Cercignani (1988) used kinetic theory to propose a "wall-function" that scaled with the mean free path. This introduces a function that complements the constitutive relations, effectively modifying the viscosity, and is able to capture some non-equilibrium behavior of the Knudsen layer. This idea has been adopted and extended (e.g. Lockerby et al. 2005; Zhang et al. 2006; Lilley and Sader 2008; Lockerby and Reese 2008; Dongari et al. 2010) with some success.

Recently, Dongari et al. (2011a) carried out molecular dynamics (MD) studies of gases and the results indicate that molecules perform Lévy-type flights under rarefied conditions, i.e. the free paths of gas molecules follow a power-law (PL) distribution. Consequently, they hypothesized that the probability distribution function for the molecular free paths of a rarefied gas followed a PL form, and this was validated against the MD data under various rarefied conditions. Using a PL distribution to describe free paths, Dongari et

al. (2011b) derived an effective MFP model for flows confined by planar surfaces by taking into account the solid boundary effects and they obtained good agreement with the MD data up to the early transition regime. In addition, they modified the Navier-Stokes constitutive relations using this PL-based MFP scaling and were then able to accurately capture the non-equilibrium effects in the Knudsen layer for isothermal pressure-driven gas flows between planar parallel walls.

A fundamental non-planar test case concerns the flow between two concentric cylinders. This is a classical fluid dynamics problem that is treated for the no-slip case in many well-known textbooks (e.g. Schlichting 1979). However, under certain conditions, the flow between the cylinders can exhibit highly non-intuitive behavior. For example, if the outer cylinder is stationary and the inner cylinder is rotating, it is possible for the velocity profile to become *inverted* i.e. the velocity will *increase* from the inner to the outer cylinder wall. This unusual phenomenon was first predicted by Einzel et al. (1990) for the case of liquid helium. Tibbs et al. (1997) extended the analysis to the case of a rarefied gas and, using DSMC, demonstrated that velocity inversion could occur provided the tangential momentum accommodation coefficient (TMAC) for the surfaces was small. (See Agrawal and Prabhu 2008a, and Agrawal and Prabhu 2008b for detailed reviews on TMAC values.) This early work has led to a number of important curvature studies for rotating Couette flow (e.g. Aoki et al. 2003; Lockerby et al. 2004; Barber et al. 2004; Yuhong et al. 2005; Myong et al. 2005; Kim 2009; Guo et al. 2011) and oscillating Couette flow (Emerson et al. 2007). These confirmed the existence of velocity inversion for small values of the TMAC and also showed that the phenomenon could be related to a critical accommodation coefficient. Indeed, Yuhong et al. (2005) derived an analytical criterion for the critical accommodation coefficient and also showed that velocity inversion was solely dependent on the value of the TMAC associated with the outer cylinder.

In this paper, we build on the approach of Dongari et al. (2011b and 2011c) and derive a PL-based effective MFP model for non-planar surfaces by incorporating the effects of curvature. We develop a curvature-dependent MFP solution for both convex and concave surfaces, and extend this analysis to deduce the effective MFP for a gas confined between two concentric cylinders. In addition, constitutive relations and velocity-slip boundary conditions are modified in accordance with the kinetic theory of gases, and tested for the classical case of isothermal rarefied Couette flow between two concentric rotating cylinders. The modified governing equations are solved for low-speed gas flows, and semi-analytical solutions are derived for the velocity profiles and the critical accommodation coefficient for velocity inversion. Our PL model results are compared with an existing slip model (Yuhong et al. 2005), the linearized BGK solution (Aoki et al. 2003), and DSMC data (Tibbs et al. 1997; Stefanov et al. 2006). We show that our PL model captures important non-linear trends associated with the physics of cylindrical Couette gas flows in the transition regime.

2 Geometry-dependent molecular mean free path

We consider a homogeneous gas, where molecules moving at an average speed $\overline{v}$ and experiencing an inter-molecular collision rate of $\dot{\theta}_v$ have a molecular mean free path $\lambda = \overline{v}/\dot{\theta}_v$. Kinetic theory-based classical expressions for the probability distribution of the free paths and the mean free path are, respectively (Kennard 1938):

$$\psi(r) = \frac{1}{\lambda} \exp\left(-\frac{|r|}{\lambda}\right), \tag{1}$$

$$\lambda = \frac{m/N_{Av}}{\pi \rho \delta^2 \sqrt{2}}, \tag{2}$$

where $|r|$ is the distance, given by $\overline{v}t$, that has been traveled by a molecule at time t, $N_{Av} = 6.0221415 \times 10^{23}$ is Avogadro's number, m is the mass of a molecule, ρ is the gas density, and δ is the hard-sphere diameter of the gas molecules.

MD results (Dongari et al. 2011a) show that the exponential distribution function for free paths (Eq. 1) is only valid when the gas is in thermodynamic equilibrium. Under non-equilibrium conditions, the MD data exhibit long-tail behavior (i.e. molecules perform Lévy-type flights) whereas the exponential distribution has a faster decay. Montroll and Scher (1973) pointed out that a finite moment of the probability distribution function implies an exponential character of the randomness. Results obtained using exponential forms of the distribution functions are applicable only to homogeneous media at equilibrium. A distribution function with diverging higher-order moments (such as the standard deviation) is essential to describe non-equilibrium transport (Montroll and Scher 1973). Instead of the classical exponential form of distribution function, Dongari et al. (2011a, 2011b) have recently hypothesized the following power-law form for the free path distribution function for a non-equilibrium gas MFP, which satisfies the requirements for diverging higher-order moments:

$$\psi(r) = B(a + r)^{-n}, \tag{3}$$

where a and B are constants with positive values that are determined through the zero and first moments. The range of values for the exponent n can be obtained by making one of the higher-order moments divergent. Zero and first moments are given as follows:

$$1 = \int_0^\infty B(a + r)^{-n} dr, \tag{4}$$

$$\lambda = \int_0^\infty Br(a + r)^{-n} dr. \tag{5}$$

Equation 4 requires the probability to range from zero to one while Eq. 5 defines the unconfined, conventional MFP value, λ. It then follows that

$$B = (n - 1)a^{n-1}, \tag{6}$$

and

$$a = \lambda(n - 2). \tag{7}$$

To develop an expression for the effective mean free path, we have adopted the approach proposed by Dongari et al. (2011b), based on an integral form of the probability distribution function, i.e.

$$p(r) = \int_0^r \psi(r)dr = \left[1 - \left(1 + \frac{r}{a}\right)^{1-n}\right], \tag{8}$$

where $p(r)$ describes the probability a molecule travels a distance r without experiencing a collision.

The probability distribution function has to be real and positive and thus $a > 0$ and $n > 2$. As $n \to \infty$, the distribution function will have finite moments, which is the condition required of an equilibrium distribution function. For a finite n, the distribution function describes a system deviating from equilibrium. So n acts as a decisive parameter to define the extent of the deviation from equilibrium. If we require the ith moment to be diverging, then $n_{max} = i + 1$. In the current paper, all our power-law (PL) model results have been obtained for $n = 3$, unless otherwise explicitly stated. Dongari et al. (2011a) validated the PL free path distribution function (Eq. 3) with MD simulations under various rarefied conditions.

Following a similar approach to that adopted by Dongari et al. (2011b), here we derive an effective mean free path model for non-planar surfaces based on a PL form of the free path distribution. Our model is derived for two generalized non-planar cases: (i) gas around a cylinder of radius R_1, i.e. a surface with convex curvature, and (ii) gas inside a cylinder of radius R_2, i.e a surface with concave curvature. Both convex and concave curvature models are then used to deduce an effective MFP model for gas confined between concentric cylinders.

In the following discussion (also see Figure 5) we use the notation R^- if a test molecule is placed above a cylinder/surface with convex curvature, and R^+ if the molecule is placed inside the cylinder/surface with concave curvature. We also use the notations θ^- and θ^+ for the equally probable zenith angle traveling direction of the molecule, towards convex and concave surfaces, respectively.

2.1   Gas outside a solid cylinder

Figure 1a presents the situation of a gas molecule outside a solid cylinder of radius, R_1, at a distance r from the center of the cylinder. The traveling distance limit for a molecule traveling towards the cylinder is denoted R_u^-, and this is associated with a critical limit for θ^- defined as θ_u^-, above which the molecule passes the cylinder and travels back into the bulk. This angle can be calculated by using the geometry of a formed right-angled triangle,
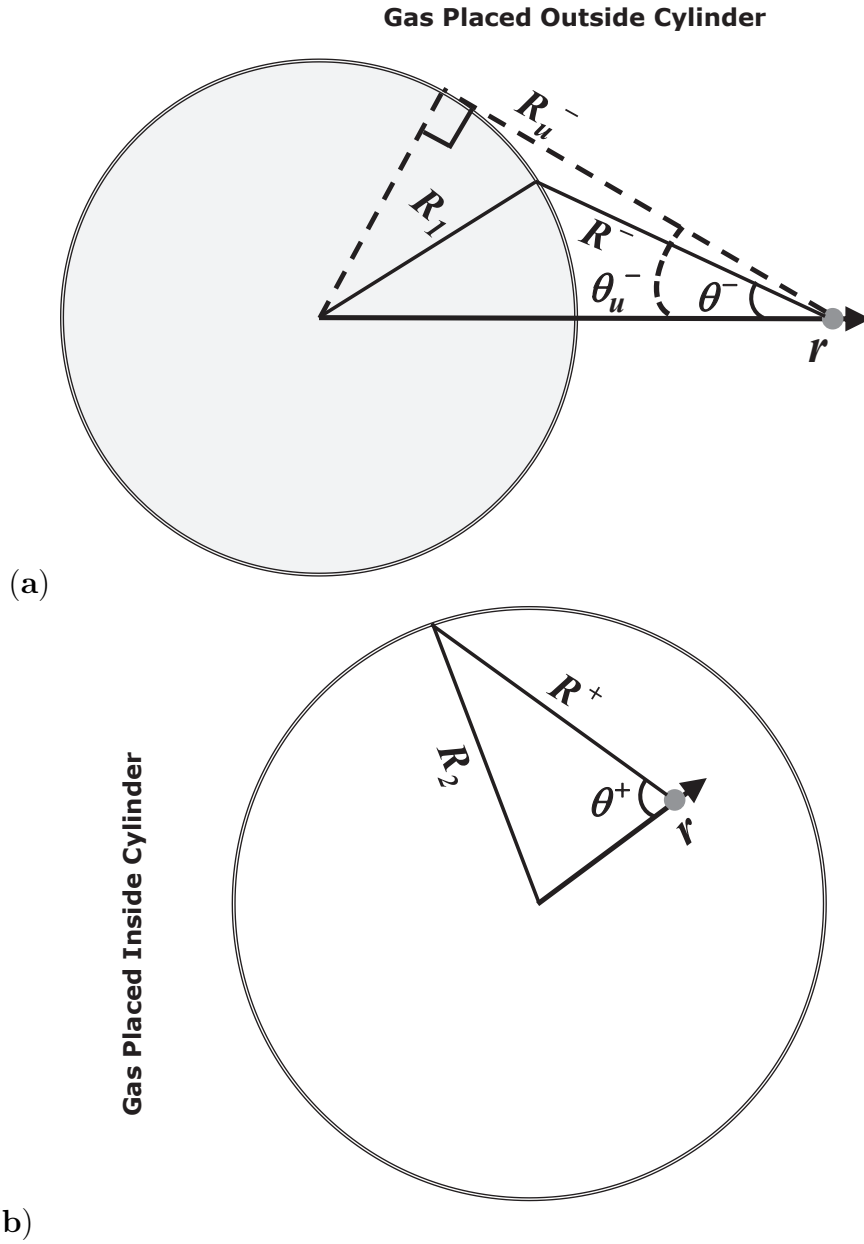
Gas Placed Outside Cylinder

(a)

Gas Placed Inside Cylinder

(b)

Figure 1: **(a)** A gas molecule outside a solid cylinder and situated at a radial distance r from the centre of the cylinder of radius R_1. R^- is the travelling distance limit for a molecule moving towards the cylinder surface, for a given zenith angle θ^-. The largest travelling distance R_u^- is achieved for the zenith angle direction θ_u^-, above which the molecule by-passes the cylinder surface and travels into the bulk. **(b)** A gas molecule inside a cylindrical cavity of radius R_2, at a wall normal distance of $R_2 - r$, where r is the radial distance of the molecule from the centre of the cylinder. The molecule has a traveling distance of R^+ to the wall for a traveling direction of θ^+, where θ^+ is varied from 0 to π.

6

with its right angle at the point connecting the radius of the cylinder and R_u^- which is tangential to the cylinder. The following relation can then be found:

$$r^2 = R_1^2 + \left(R_u^-\right)^2. \tag{9}$$

By using the relation $R_1 = r \sin(\theta_u^-)$, the value of θ_u^- is obtained as:

$$\theta_u^- = \arcsin\left(\frac{R_1}{r}\right). \tag{10}$$

The distance of the molecule away from the cylinder surface, R^-, as a function of θ^-, can be determined in terms of r and R_1 by using the cosine law:

$$R_1^2 = r^2 + (R^-)^2 - 2rR^-\cos(\theta^-), \tag{11}$$

which is a simple quadratic in R^-, whose root is given by

$$R^-(r, \theta^-) = r\cos(\theta^-) - \sqrt{(r\cos(\theta^-))^2 + R_1^2 - r^2}. \tag{12}$$

The average distance a molecule travels to the cylinder's surface, with respect to the angle θ^-, is achieved by the following integral mean value theorem:

$$\langle R^- \rangle = \frac{1}{\Omega} \int_0^\Omega R^-(r, \theta^-) d\theta^-, \tag{13}$$

where Ω is the solid angle subtended by the cylinder at a point in the base plane, at a distance r ($> R_1$) from the axis of the cylinder of length L, and which can be expressed as (Guest 1960):

$$\Omega = \theta_u^- - \frac{1}{2}\left[\left(\left(\frac{r}{R_1}\right)^2 - 1\right)^{\frac{1}{2}} + \theta_u^- - \frac{\pi}{2}\right] L^{-2} + O\left(L^{-4}\right). \tag{14}$$

If we consider the length of the cylinder L tending to infinity, then Ω can be simplified to

$$\Omega = \theta_u^-. \tag{15}$$

Using Eq. 8, the mean free path of the molecules traveling in the direction of the cylinder (a surface with convex curvature) is then,

$$\lambda_{\text{eff(conv)}} = \lambda \left[1 - \frac{1}{\theta_u^-} \int_0^{\theta_u^-} \left(1 + \frac{R^-(r, \theta^-)}{a}\right)^{(1-n)} d\theta^-\right]. \tag{16}$$

The general mean free path expression is obtained by considering all possible molecular traveling directions. This is achieved in a similar manner to the analysis for a gas confined between planar parallel walls presented by Dongari et al. (2011b). In the case of planar parallel walls, it is equally probable that a molecule travels towards one surface or the other.

In the present case, solid angle theory is used to determine the likelihood of a molecule traveling in the direction of the cylinder, as opposed to traveling towards the bulk; the probabilities being expressed as θ_u^-/π and $[1 - (\theta_u^-/\pi)]$, respectively. From this weighting, the general expression for the effective mean free path of a gas placed outside a cylinder is:

$$\lambda_{\text{eff(o)}} = \lambda_{\text{eff(conv)}} \left(\frac{\theta_u^-}{\pi} \right) + \lambda \left[1 - \left(\frac{\theta_u^-}{\pi} \right) \right], \tag{17}$$

where λ is the unconfined mean free path. This equation can also be written as $\lambda_{\text{eff(o)}} = \lambda \, \beta_{(o)}(r, R_1/\lambda)$, where

$$\beta_{(o)} = \left(\frac{\theta_u^-}{\pi} \right) \left[1 - \frac{1}{\theta_u^-} \int_0^{\theta_u^-} \left(1 + \frac{R^-(r, \theta^-)}{a} \right)^{(1-n)} d\theta^- \right] +$$
$$\left[1 - \left(\frac{\theta_u^-}{\pi} \right) \right], \tag{18}$$

which is the normalized effective MFP based on a power-law distribution function, where the subscript (o) denotes our considerations of gas molecules *outside* a cylindrical surface. It should be noted that a is dependent on the mean free path (see Eq. 7) and $r \geq R_1$, as the gas is outside the cylinder. For a given angle, Eq. 18 is dependent on r, R_1 and λ, and can be evaluated as a function of the non-dimensional wall-normal distance $[(r - R_1)/\lambda]$, for a given $b_1 = R_1/\lambda$, the inverse of the normalized curvature. As $b_1 \to \infty$, the solution of Eq. 18 should reduce to the planar case. Equation 18 can be computed numerically using Simpson's rule; in the present study, we have used 16 subintervals.

The solution of the effective mean free path for a convex surface must reduce to that for a planar one-wall case when the radius of the cylinder tends to infinity. To verify this limiting case, the normalized effective MFP solutions (i.e. $\beta_{(o)}$) from Eq. 18, are plotted in Fig. 2 for various values of b_1 and are compared with the planar one-wall solution derived by Dongari et al. (2011b). For a value of $b_1 = 3$, the non-planar solution predicts a higher β value at the surface and also exhibits a sharper gradient compared to the planar one-wall case. Figure 2 shows that, as the radius R_1 of the cylinder increases, our non-planar solution tends to the planar solution.

2.2   Gas inside a hollow cylinder

Using a similar approach, it is possible to obtain the effective mean free path for gas molecules inside a hollow cylinder of radius R_2, i.e. for a surface with a concave curvature. As illustrated in Fig. 1b, r is a target molecule's radial distance from the centre of the cylinder and R^+ is the molecule's distance to the wall if the molecule has a traveling trajectory of θ^+.
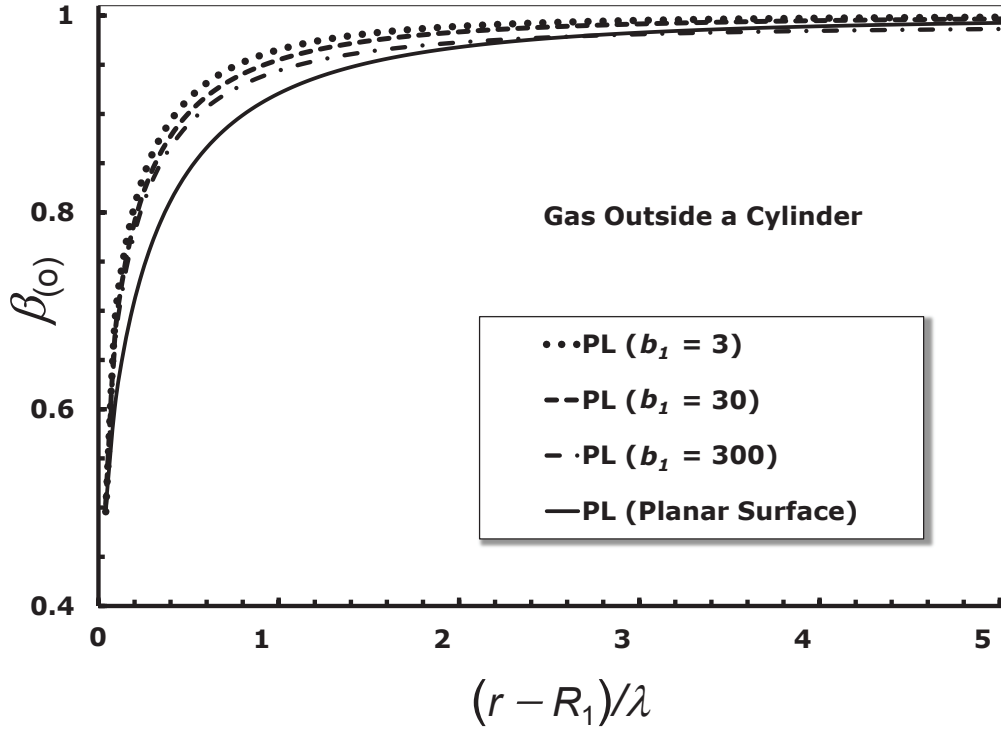
Figure 2: Variation of the effective mean free path of gas molecules outside a solid cylinder (surface with a convex curvature) as a function of non-dimensional wall-normal distance $[(r - R_1)/\lambda]$. Here, $r \geq R_1$, as the gas is placed outside the cylinder and on the x-axis, r is varied by fixing R_1 and λ, for a given value of b_1. The MFP profiles for various values of b_1 (R_1/λ) are illustrated to show the effect of the convex curvature and their comparison with the planar one-wall solution (Dongari et al. 2011b).

To calculate the effective mean free path, the wall distance of the molecule has first to be calculated using the cosine law:

$$R_2^2 = r^2 + (R^+)^2 - 2rR^+\cos(\theta^+), \qquad (19)$$

where the molecule's traveling trajectory θ^+ can vary from 0 to π. The molecular traveling distance to the wall, R^+, depends on r and θ^+ and can be expressed as:

$$R^+(r, \theta^+) = -r\cos(\theta^+) + \sqrt{(r\cos(\theta^+))^2 + R_2^2 - r^2}. \qquad (20)$$

The solid angle subtended by the cylinder at a point lying inside the cylinder is 2π. Using quarter symmetry, it is sufficient to integrate θ^+ from 0 to $\pi/2$. Using our PL distribution to describe the molecular free paths (Eq. 8), the expression for the effective mean free path of a gas molecule inside a cylinder (i.e. interacting with a surface with concave curvature) is:

$$\lambda_{\text{eff(conc)}} = \lambda \left[1 - \frac{2}{\pi} \int_0^{\pi/2} \left(1 + \frac{R^+(r, \theta^+)}{a} \right)^{(1-n)} d\theta^+ \right], \qquad (21)$$

or the normalized expression:

$$\beta_{(i)} = \frac{\lambda_{\text{eff(conc)}}}{\lambda} = 1 - \frac{2}{\pi} \int_0^{\pi/2} \left(1 + \frac{R^+(r, \theta^+)}{a} \right)^{(1-n)} d\theta^+, \qquad (22)$$

where the subscript (i) denotes that the gas molecules are located *inside* the cylinder. Equation 22 is dependent on r, R_2 and λ, and can be evaluated as a function of the non-dimensional wall-normal distance $[(R_2 - r)/\lambda]$, for a given $b_2 = R_2/\lambda$. Here $r \leq R_2$, as the gas is inside the cylinder.

In a similar manner to the convex case, the effective MFP solution for a concave surface must also reduce to the planar one-wall case when the radius of the cylinder tends to infinity. Figure 3 shows the variation of the normalized effective mean free path $\beta_{(i)}$, for various b_2 values and a comparison with the planar one-wall solution (Dongari et al. 2011b). For a value of $b_2 = 5$, the non-planar solution predicts a lower β value at the surface and exhibits a shallower gradient compared to the planar case. For higher values of b_2, the non-planar concave solution approaches the planar case. However, at the surface, even for $b_2 = 30$, the non-planar solution predicts a lower value of $\beta_{(i)} \sim 0.4691$ compared to the corresponding planar wall value of 0.5. This is due to the concave nature of the surface, where a molecule will encounter more frequent collisions with the wall.

2.3   Gas confined between concentric cylinders

We now consider a gas between two concentric cylinders, with R_1 and R_2 being the radii of the inner and outer cylinders, respectively. Let us consider a molecule situated at a distance
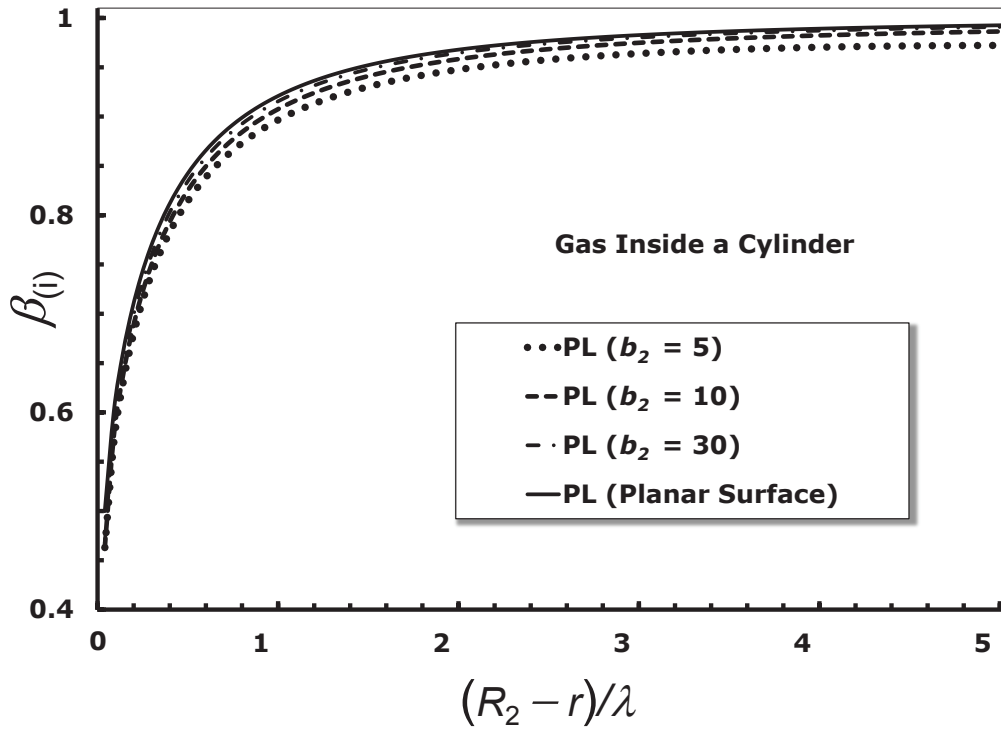
Figure 3: Variation of the effective mean free path of a gas molecule inside a cylinder (i.e. a bounding surface with concave curvature) as a function of non-dimensional wall-normal distance $[(R_2 - r)/\lambda]$. Here, $r \leq R_2$, as the gas is placed inside the cylinder and on the x-axis, r is varied by fixing R_2 and λ, for a given value of b_2. The MFP profiles for various values of b_2 (R_2/λ) are illustrated to show the effect of the concave curvature and their comparison with the planar one-wall solution (Dongari et al. 2011b).

r from the coincident centres of the two cylinders. The inner cylinder presents a surface with convex curvature (Fig. 1a) to the molecule and the outer cylinder presents a surface with a concave curvature (Fig. 1b). The probability of a molecule traveling towards the inner and outer cylinder directions can be evaluated as θ_u^-/π and $[1 - (\theta_u^-/\pi)]$, respectively. Using Eqs. 16 and 21 and accounting for this weighting, the complete expression for the effective mean free path of a gas confined between two concentric cylinders is:

$$\lambda_{\text{eff}} = \lambda_{\text{eff(conv)}} \left(\frac{\theta_u^-}{\pi} \right) + \lambda_{\text{eff(conc)}} \left[1 - \left(\frac{\theta_u^-}{\pi} \right) \right], \tag{23}$$

where we can then write $\lambda_{\text{eff}} = \lambda \, \beta$, so

$$\beta = \left(\frac{\theta_u^-}{\pi} \right) \left[1 - \frac{1}{\theta_u^-} \int_0^{\theta_u^-} \left(1 + \frac{R^-(r, \theta^-)}{a} \right)^{(1-n)} d\theta^- \right] +$$
$$\left[1 - \left(\frac{\theta_u^-}{\pi} \right) \right] \left[1 - \frac{1}{\theta_u^+} \int_0^{\theta_u^+} \left(1 + \frac{R^+(r, \theta^+)}{a} \right)^{(1-n)} d\theta^+ \right], \tag{24}$$

with

$$\theta_u^+ = \pi - \theta_u^-. \tag{25}$$

Here, β is the geometry-dependent MFP based on a power-law distribution function and is dependent on the Knudsen number, Kn, through the mean free path, λ, and a geometry constraint, R_2/R_1. The Knudsen number is defined as:

$$Kn = \frac{\lambda}{R_2 - R_1}. \tag{26}$$

Figure 4a shows the variation of β between the inner and outer cylinders (with $R_2/R_1 = 5/3$) for various Knudsen numbers in the slip and early transition regimes. The MFP profiles are sharper at the inner cylinder and shallower at the outer cylinder and they are not symmetric about the midpoint of the gap between the cylinders. This finding is in contrast to the solution for the planar parallel wall case, where the MFP profile is symmetric about the midpoint of the gap between the surfaces (Dongari et al. 2011b). The anti-symmetric effect increases with Knudsen number. The values of β are relatively high at the inner cylinder surface compared to the outer cylinder, due to the convex and concave curvature effects, respectively. The difference in the values of β at the inner and outer cylinders is also dependent on the Knudsen number.

To illustrate further the curvature effects, Fig. 4b presents the ratio of the effective MFPs from the non-planar and planar cases. The non-planar values, β_{NP}, are obtained from Eq. 24 for $R_2/R_1 = 5/3$ and β_{P}, for the case of planar parallel walls, is evaluated using Eq. 12 in Dongari et al. (2011b). For $Kn = 0.01$, the curvature effects are negligible, except in a thin layer close to the surface of the outer cylinder. As the Knudsen number
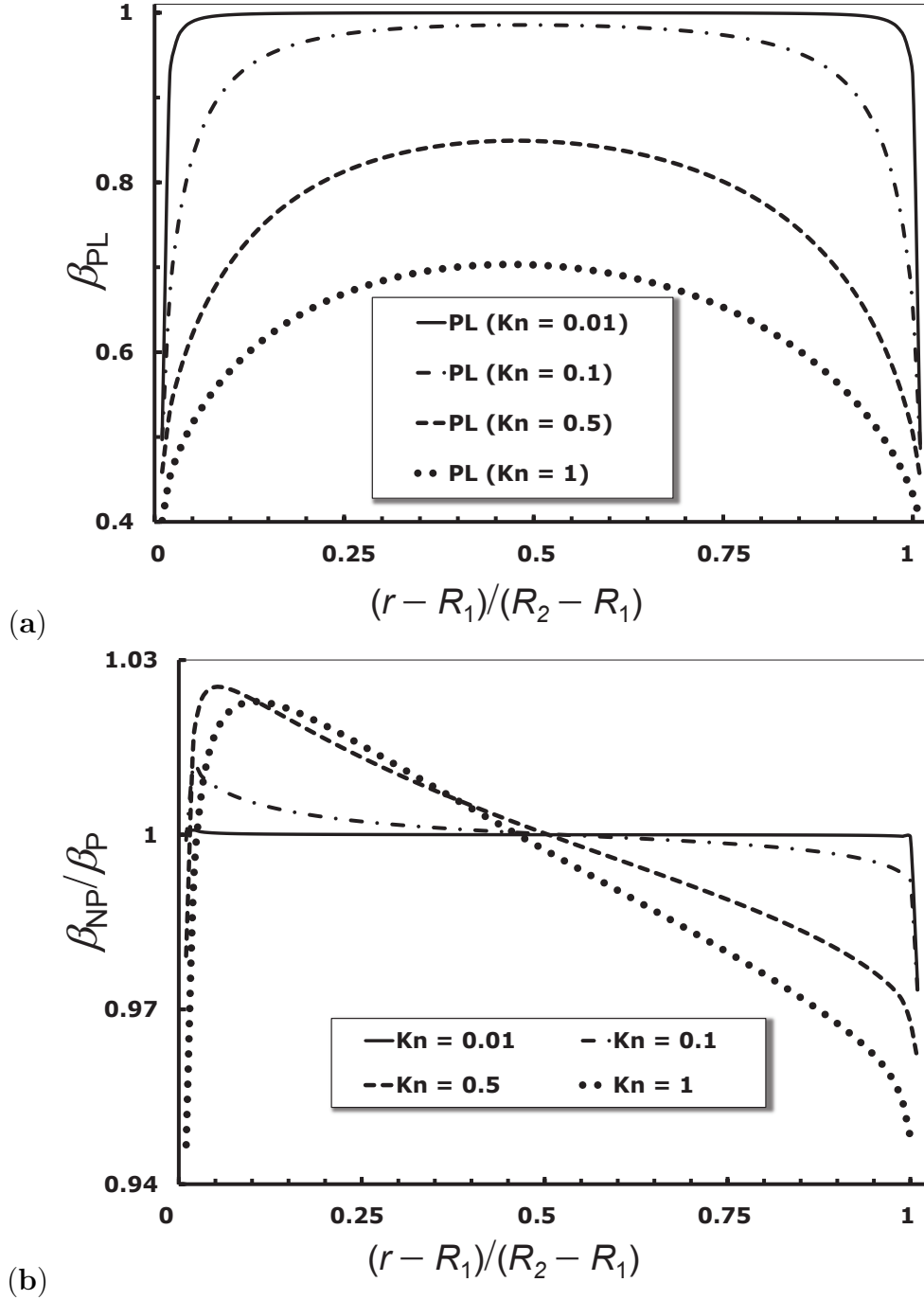
Figure 4: (a) Variation of β with normalized radial distance $(r - R_1)/(R_2 - R_1)$ between two concentric cylinders with $R_2/R_1 = 5/3$ for various Knudsen numbers in the slip and transition regimes. (b) Illustration of curvature effects through the ratio of the MFP values for a gas confined between non-planar (NP) and planar (P) surfaces. The non-planar solution is obtained from Eq. 24 and the planar solution is computed using Eq. 12 in Dongari et al. (2011b).

increases, both the curvature and anti-symmetric effects become more pronounced, whereas the difference in the values of β at the inner and outer cylinders decreases. The ratio $\beta_{\mathrm{NP}}/\beta_{\mathrm{P}}$ has its minimum at the outer cylinder for all Kn and its maximum at a position close to the surface of the inner cylinder. However, this point moves away from the inner cylinder with increasing Kn as the thickness of the Knudsen-layer increases.

3 Cylindrical Couette flow

3.1 Problem description and governing equations

To evaluate our PL-based effective MFP scaling for non-planar cases, we consider a rarefied gas confined between two concentric rotating cylinders as shown in Fig. 5. The flow is assumed to be fully developed, two-dimensional, isothermal, laminar and steady, with a low Reynolds number (Re) so that inertial effects may be neglected.

With these assumptions, the governing flow equation in cylindrical coordinates is

$$\frac{1}{r^2}\frac{d}{dr}\left(r^2\tau_{r\phi}\right) = 0, \tag{27}$$

where r is the radial coordinate, ϕ is the tangential coordinate, and $\tau_{r\phi}$ is the tangential stress which is defined as:

$$\tau_{r\phi} = \mu\left(\frac{du_\phi}{dr} - \frac{u_\phi}{r}\right), \tag{28}$$

where μ is the fluid dynamic viscosity and u_ϕ is the velocity of the fluid in the tangential direction.

From the kinetic theory of gases, the fluid viscosity can be explained in terms of the collisions between gas molecules, and of the free paths which the molecules describe between collisions. The unconfined MFP is then related to the shear viscosity (Cercignani 1988):

$$\mu = \rho\frac{\lambda}{\sqrt{\pi/2RT}}, \tag{29}$$

where ρ is the gas density, R is the specific gas constant, and T the gas temperature.

Equation 29 is only valid for flows that are in quasi-equilibrium. Within the Knudsen layer, the flight paths of the gas molecules are affected by the presence of a solid wall. If we wish to use Eq. 29, we need to take into account the MFP affected by gas molecular collisions with surfaces. If the unconfined expression for the MFP, λ, is replaced by our effective and geometry-dependent mean free path, λ_{eff} (Eqs. 23 and 24), we obtain a non-constant, geometry-dependent, effective viscosity, μ_{eff}, that can then be used to deduce a
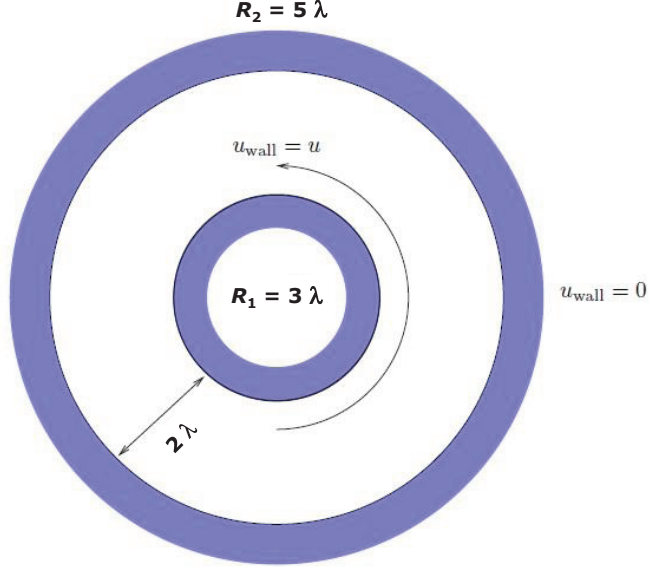
Figure 5: Schematic of Couette flow between concentric rotating cylinders.

non-linear stress/strain-rate relation:

$$\tau_{r\phi} = \underbrace{\mu\beta}_{\mu_{\text{eff}}} \left(\frac{du_\phi}{dr} - \frac{u_\phi}{r} \right). \tag{30}$$

Substituting Eq. 30 into Eq. 27 results in the modified governing equation:

$$\frac{\mu}{r^2} \frac{d}{dr} \left[r^2 \beta \left(\frac{du_\phi}{dr} - \frac{u_\phi}{r} \right) \right] = 0. \tag{31}$$

This needs to be solved in conjunction with the following slip boundary conditions at the inner and outer cylinder surfaces, respectively:

$$u_\phi|_{r=R_1} = \omega_1 R_1 + \underbrace{\frac{2-\sigma_1}{\sigma_1}}_{\alpha_1} \lambda \left[\beta \left(\frac{du_\phi}{dr} - \frac{u_\phi}{r} \right) \right] \Bigg|_{r=R_1}, \tag{32}$$

$$u_\phi|_{r=R_2} = \omega_2 R_2 - \underbrace{\frac{2-\sigma_2}{\sigma_2}}_{\alpha_2} \lambda \left[\beta \left(\frac{du_\phi}{dr} - \frac{u_\phi}{r} \right) \right] \Bigg|_{r=R_2}, \tag{33}$$

where ω_1 and ω_2 are the angular velocities and σ_1 and σ_2 are the tangential moment accommodation coefficients of the inner and outer cylinders, respectively.

The solution for the velocity profile can then be obtained as:

$$u_\phi(r) = r \left[\omega_1 + \frac{\alpha_1 \lambda C}{R_1^3} + G(r)C \right], \tag{34}$$

where

$$G(r) = \int_{R_1}^{r} \frac{dr}{r^3 \beta}, \tag{35}$$

$$C = \frac{\omega_2 - \omega_1}{\left[H + \frac{\alpha_1 \lambda}{R_1^3} + \frac{\alpha_2 \lambda}{R_2^3} \right]}, \tag{36}$$

$$H = \int_{R_1}^{R_2} \frac{dr}{r^3 \beta}. \tag{37}$$

When the effects of the Knudsen layer are neglected, i.e. the mean free path has no geometry dependence, then Eq. 34 simply reduces to the velocity profile based on the classical slip solution, as presented in Eq. 6 of Yuhong et al. (2005).

3.2 Results and discussion

To illustrate the phenomenon of velocity inversion, in the present study the outer cylinder is kept stationary ($\omega_2 = 0$) and the inner cylinder is allowed to rotate. The radii of the inner and outer cylinders are chosen to be 3λ and 5λ, respectively, making $Kn = 0.5$, and the accommodation coefficients are initially assumed to be equal at the inner and outer surfaces ($\sigma_1 = \sigma_2 = \sigma$). Figure 6a presents a comparison between our solution based on the PL effective MFP (Eq. 34) and the DSMC data reported by Tibbs et al. (1997). The PL model is in very good quantitative agreement with the DSMC results for the $\sigma = 1.0$ and 0.7 cases. The results show that the DSMC data and PL formulation follow the same basic trends and predict an inverted velocity profile when the accommodation coefficient is 0.1. However, slight deviations are discernible at the surface of the outer cylinder for the $\sigma = 0.4$ and 0.1 cases.

It is interesting to note that, for the specific case when the accommodation coefficients of the inner and outer cylinders are the same, the family of velocity profiles all pass through a common point that is independent of the value of the accommodation coefficient. This intersection point in the PL profiles is fairly close to the point predicted by the DSMC data, whereas the classical slip solution predicts this point closer to the outer cylinder, as shown in Fig. 6b. The classical slip solution is unable to account for any variation in MFP and fails to capture non-linear effects associated with the Knudsen layers at the inner and outer cylinders. The discrepancies are greatest when $\sigma = 1.0$ but decrease as σ is reduced. At very low values of σ, the PL and classical slip solutions are identical and yield the same solid body rotation solution as $\sigma \to 0$.

Figure 7 shows the case when the accommodation coefficient of the inner cylinder is maintained at unity ($\sigma_1 = 1.0$) whilst the accommodation coefficient of the outer cylinder (σ_2) is varied from 0.02 to 0.3. Normal (non-inverted), fully inverted and partially inverted velocity profiles are seen in both the PL model results and our new DSMC data. For the present study, we have adopted the standard DSMC algorithm originally proposed by

16
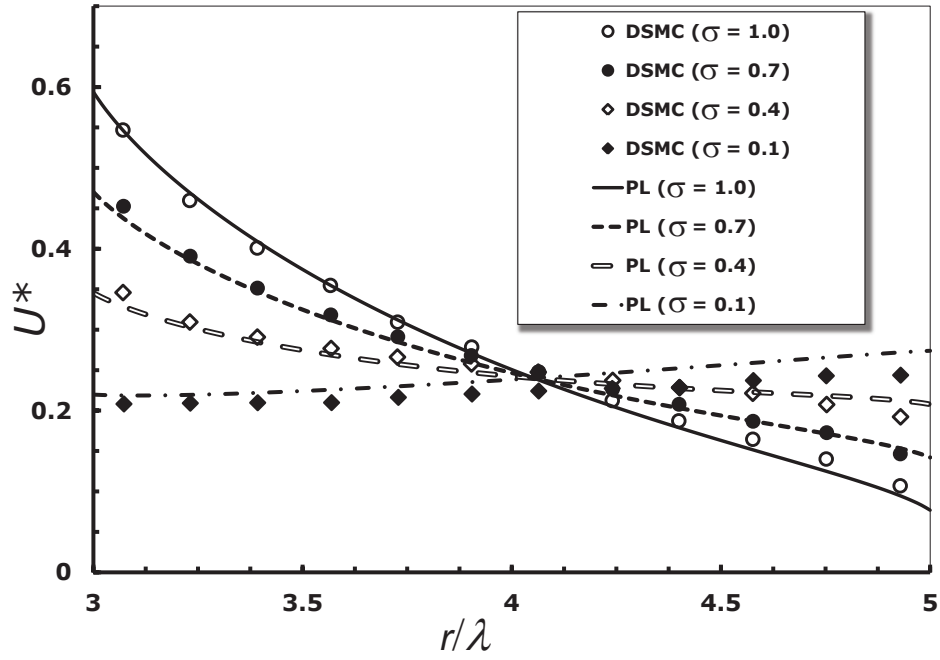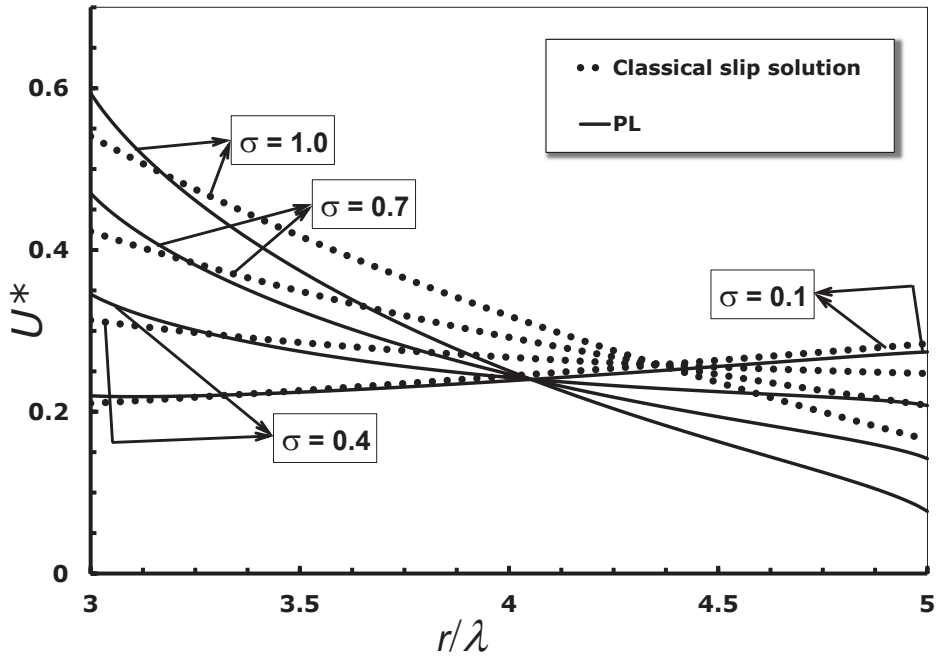
Figure 6: Variation of the non-dimensional velocity $[U^* = u_\phi/(\omega_1 R_1)]$ as a function of the radial distance for cylindrical Couette flow with $\sigma_1 = \sigma_2 = \sigma$. Comparison of PL model results against (**a**) DSMC data (Tibbs et al. 1997) and (**b**) the classical slip solution (Yuhong et al. 2005). The results are presented for $Kn = 0.5$ and $R_2/R_1 = 5/3$.

Bird (1994), with a small modification in the calculation of the maximum collision number in a cell, as described by Stefanov et al. (1998). Weighting factors for improving the particle number balance in the radial direction were not included in the present algorithm since the simulations did not consider large ratios of cylinder radii (Emerson et al. 2007). The present simulations employed a hard-sphere model for argon at STP conditions with isothermal boundary conditions. The one-dimensional computational domain between the cylinders was discretized using a uniform distribution of cells in the radial direction with a typical grid resolution of 100 cells across the annular gap.

For the partially inverted cases in Fig. 7, both the PL model and the DSMC data predict an initial decrease in velocity away from the inner cylinder, then an increase towards the outer cylinder, and then another decrease in a very thin layer close to the surface of the outer cylinder. This is in contrast to the predictions of the classical slip solution (Yuhong et al. 2005) where the velocity profile has an initial decrease away from the inner cylinder and then just an increase towards the outer cylinder. Our PL model is able to predict the non-linear effects quite well, except very close to the surface of the outer cylinder, where the DSMC data exhibit a sharp decrease in the velocity, which is not captured by our model. Quantitative agreement with the DSMC data is good for $\sigma_2 > 0.2$ and $\sigma_2 < 0.1$. The PL model exhibits a conventional velocity profile up to $\sigma_2 \sim 0.25$ and below that it shows a partially inverted profile up to $\sigma_2 \sim 0.10$, whereas for the classical slip solution the corresponding values are 0.4 and 0.2, respectively.

As mentioned in section 2, throughout this paper the value of the power-law exponent has been fixed to $n = 3$ for all the reported results. Figure 8 demonstrates the effect of the value of n on the structure of the velocity profile in the Knudsen layer, for $\sigma_1 = 1.0$ and (a) $\sigma_2 = 1.0$, (b) $\sigma_2 = 0.4$ and (c) $\sigma_2 = 0.15$. The velocity profiles are almost unaffected by the value of n at high values of the accommodation coefficients ($\sigma_2 = 1.0$) across the entire annular clearance. However, decreasing σ_2 to 0.4, the results are sensitive to the exponent value, but only in the Knudsen layer at the outer cylinder. For small accommodation coefficients ($\sigma_2 = 0.15$), the velocity profiles are shown clearly to depend on the value of n and the sensitivity increases towards the outer cylinder.

3.3 Critical accommodation coefficients

In this section, we identify critical accommodation coefficients that produce (i) normal, (ii) fully-inverted, and (iii) partially-inverted velocity profiles. A normal (non-inverted) velocity profile occurs when the tangential velocity decreases monotonically from the inner to the outer cylinder. In contrast, a fully-inverted case occurs when the velocity monotonically increases. Finally, a partially-inverted profile occurs when there is a decrease and increase at multiple locations between the inner and outer cylinders.

The velocity profile is given in Eq. 34; the gradient of this can be used as a criterion to judge whether the function is monotonically decreasing or increasing. After some simplifi-
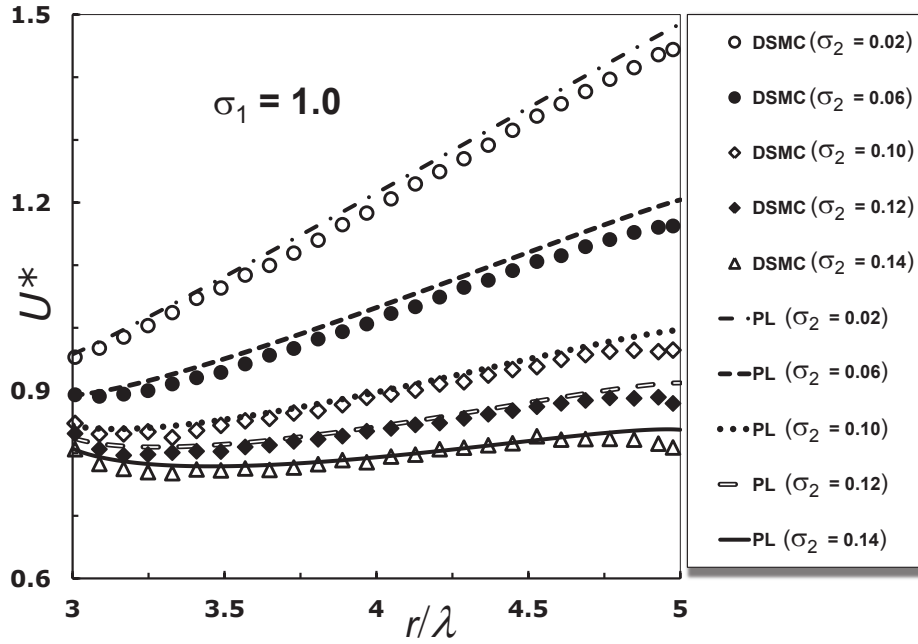
(a)
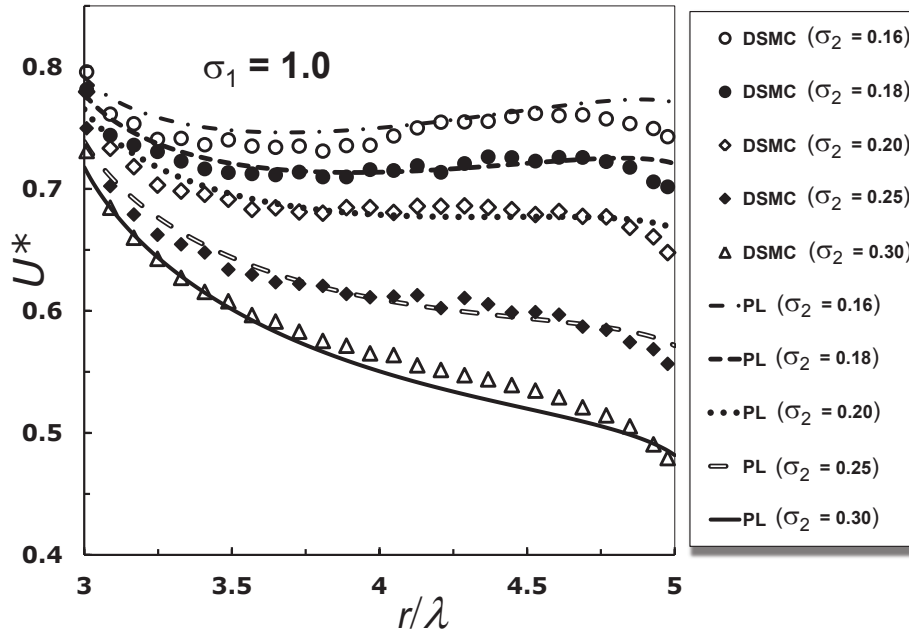
(b)

Figure 7: Variation of the non-dimensional velocity $[U^* = u_\phi/(\omega_1 R_1)]$ as a function of the radial distance for $\sigma_1 = 1.0$ and various values of σ_2, ranging from (**a**) 0.02 to 0.14 and (**b**) 0.16 to 0.30. Normal, fully-inverted and partially-inverted velocity profiles are seen in both the PL model results and the DSMC data, for $Kn = 0.5$ and $R_2/R_1 = 5/3$.
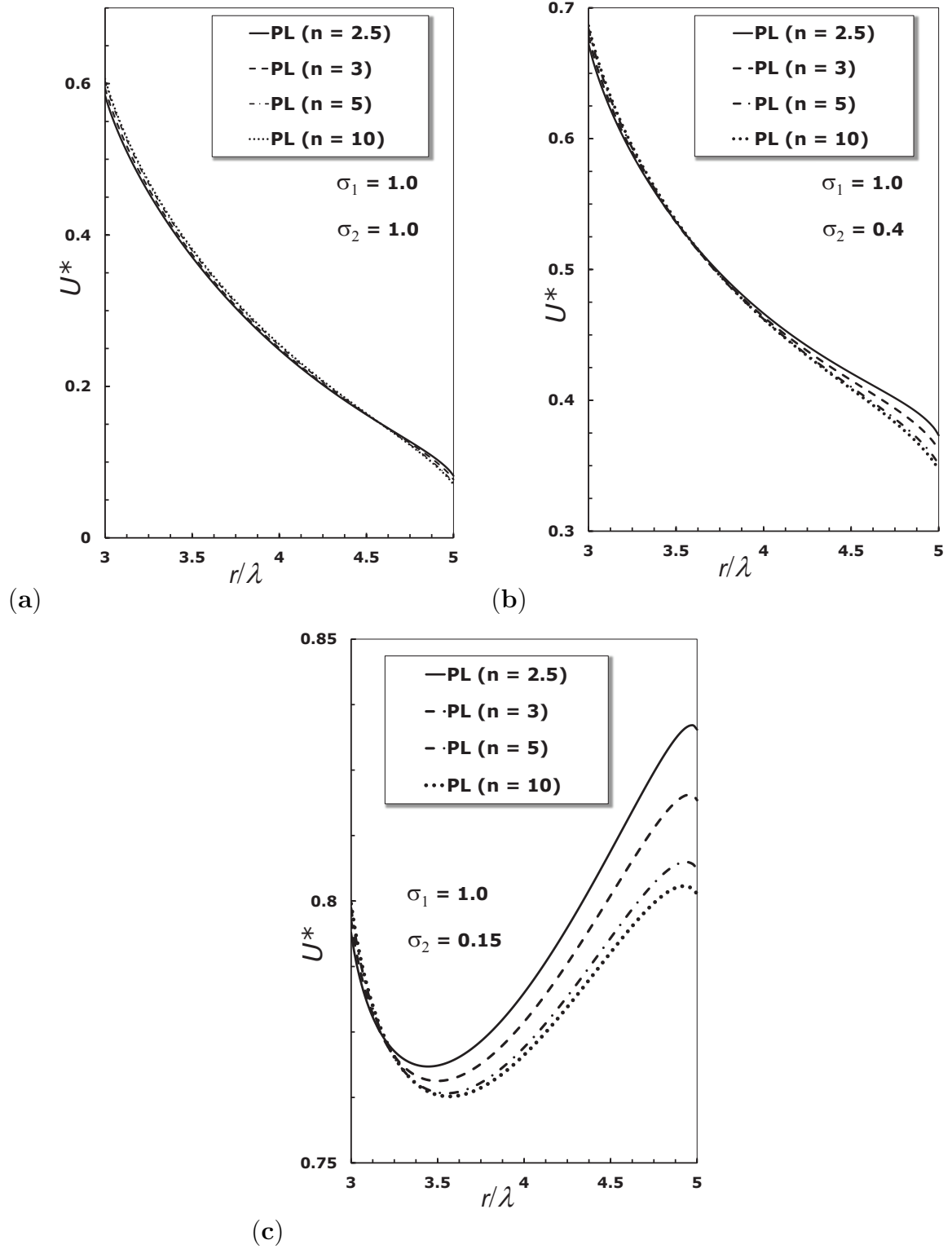
Figure 8: Effect of the power-law distribution function exponent, n, on the velocity profiles. Variation of the non-dimensional velocity $[U^* = u_\phi/(\omega_1 R_1)]$ with radial distance for $\sigma_1 = 1.0$ and (**a**) $\sigma_2 = 1.0$, (**b**) $\sigma_2 = 0.4$ and (**c**) $\sigma_2 = 0.15$, for $Kn = 0.5$ and $R_2/R_1 = 5/3$.

cations, the velocity gradient for the case of a rotating inner cylinder and stationary outer cylinder can be expressed as:

$$\frac{du_\phi}{dr} = \omega_1 \left[1 - \frac{1}{H + \frac{\alpha_1\lambda}{R_1^3} + \frac{\alpha_2\lambda}{R_2^3}} \left(\frac{\alpha_1\lambda}{R_1^3} + G(r) + \frac{1}{r^2\beta} \right) \right]. \tag{38}$$

If $du_\phi/dr > 0$, a fully inverted velocity profile exists, and this is only satisfied when:

$$\frac{\left(\frac{\alpha_1\lambda}{R_1^3} + G(r) + \frac{1}{r^2\beta} \right)}{H + \frac{\alpha_1\lambda}{R_1^3} + \frac{\alpha_2\lambda}{R_2^3}} < 1, \tag{39}$$

which can only hold throughout the annular clearance ($R_1 \leq r \leq R_2$), when $[G(r) + 1/(r^2\beta)]$ is at its maximum value, which occurs at $r = R_1$. Using this condition, the critical accommodation coefficient for a fully inverted velocity profile (i.e. positive velocity gradient) can be expressed as:

$$(\sigma_2)_{\mathrm{P}} = 2 \left[1 + \frac{R_2^3}{R_1^2\beta\lambda} - \frac{R_2^3}{\lambda}H \right]^{-1}. \tag{40}$$

Equation 40 provides an upper bound, so for $\sigma_2 < (\sigma_2)_{\mathrm{P}}$ a fully inverted velocity will always occur, and this phenomenon is independent of the value of the accommodation coefficient at the inner cylinder. In the absence of any Knudsen layer in the flow, i.e. a constant mean free path between the inner and outer cylinders, Eq. 40 simply reduces to the classical slip solution presented in Eq. 17 of Yuhong et al. (2005).

From Eq. 38, if $du_\phi/dr < 0$, the velocity will be a decreasing function of r and no inverted velocity profile will be observed. This situation can only exist when:

$$\frac{\left(\frac{\alpha_1\lambda}{R_1^3} + G(r) + \frac{1}{r^2\beta} \right)}{H + \frac{\alpha_1\lambda}{R_1^3} + \frac{\alpha_2\lambda}{R_2^3}} > 1, \tag{41}$$

which can only hold throughout the annular clearance ($R_1 \leq r \leq R_2$) when $G(r) + 1/(r^2\beta)$ is at its minimum value, which occurs for $r = r_c$ ($R_1 < r_c < R_2$). The value of r_c can be obtained numerically for a given Kn and R_2/R_1 and then the critical accommodation coefficient for no velocity inversion (i.e. negative velocity gradient) follows as:

$$(\sigma_2)_{\mathrm{N}} = 2 \left[1 + \frac{R_2^3}{R_c^2\beta(r_c)\lambda} - \frac{R_2^3}{\lambda}(G(r_c) - H) \right]^{-1} \tag{42}$$

Equation 42 provides a lower bound, so for $\sigma_2 > (\sigma_2)_{\mathrm{N}}$ no inverted velocity profile will occur and this phenomenon is also independent of the value of the accommodation coefficient at the inner cylinder, as in the case above. When there is no mean free path variation between the inner and outer cylinders, Eq. 42 reduces to the corresponding classical slip solution (see Eq. 19 of Yuhong et al. 2005).

Considering these two cases given by Eqs. 40 and 42, it is evident that a *partially-inverted* velocity profile will occur when the accommodation coefficient at the outer cylinder lies within the range:

$$(\sigma_2)_{\mathrm{P}} < \sigma_2 < (\sigma_2)_{\mathrm{N}}. \tag{43}$$

This also does not depend on the accommodation coefficient of the inner cylinder.

Figure 9a presents the variation of the critical accommodation coefficient $(\sigma_2)_{\mathrm{N}}$ as a function of Knudsen number. Our PL model results are compared with DSMC data (Stefanov et al. 2006), the classical slip solution (Eq. 19 of Yuhong et al. 2005) and the linearized BGK model (Aoki et al. 2003), in the flow regime $0 < Kn < 1$. In the continuum regime ($Kn < 0.001$), all three theoretical models converge to similar values. In the slip flow regime ($0.001 < Kn < 0.1$), the PL model lies below the classical slip solution and the BGK model. The PL model results show very good quantitative agreement with the DSMC data in the early transition regime ($0.1 < Kn < 0.5$), whereas the other two models show significant deviations. Although DSMC data are not available beyond $Kn > 0.5$, by extrapolating the trend up to $Kn = 0.5$ the PL model may slightly overpredict $(\sigma_2)_{\mathrm{N}}$ in the latter part of the transition regime. In the free-molecular regime, the PL model asymptotically reaches a constant value (~ 0.7) and both the classical slip solution and the BGK model diverge (not shown in Fig. 9a).

Figure 9b shows the variation of the critical accommodation coefficient, $(\sigma_2)_{\mathrm{P}}$, as a function of Knudsen number. Our PL model is compared with the classical slip solution (see Eq. 17 of Yuhong et al. 2005) from the slip to the free-molecular regime ($0.001 < Kn < 10$), although the continuum assumptions are highly questionable for $Kn > 1$. The classical slip solution significantly overpredicts the PL model in the transition regime and beyond. For $Kn >> 1$, the slip solution indeed shows a diverging and unphysical behavior with $(\sigma_2)_{\mathrm{P}}$ values greater than unity. Conversely, our PL model reaches a constant value of ~ 0.3.

4   Conclusions

The non-equilibrium flow physics of rarefied gases interacting with non-planar surfaces has been described using a power-law (PL) probability distribution function for the free-paths of the gas molecules. We have developed new geometry-dependent mean free path solutions for both convex and concave surfaces that take into account the termination of the free paths of gas molecules at the curved surfaces. Subsequently, a hypothetical constitutive scaling approach to model the Knudsen layer within a conventional continuum fluid dynamics framework has been proposed, in accordance with the kinetic theory of gases. This has been tested for the case of isothermal rarefied Couette flow between two concentric rotating cylinders.
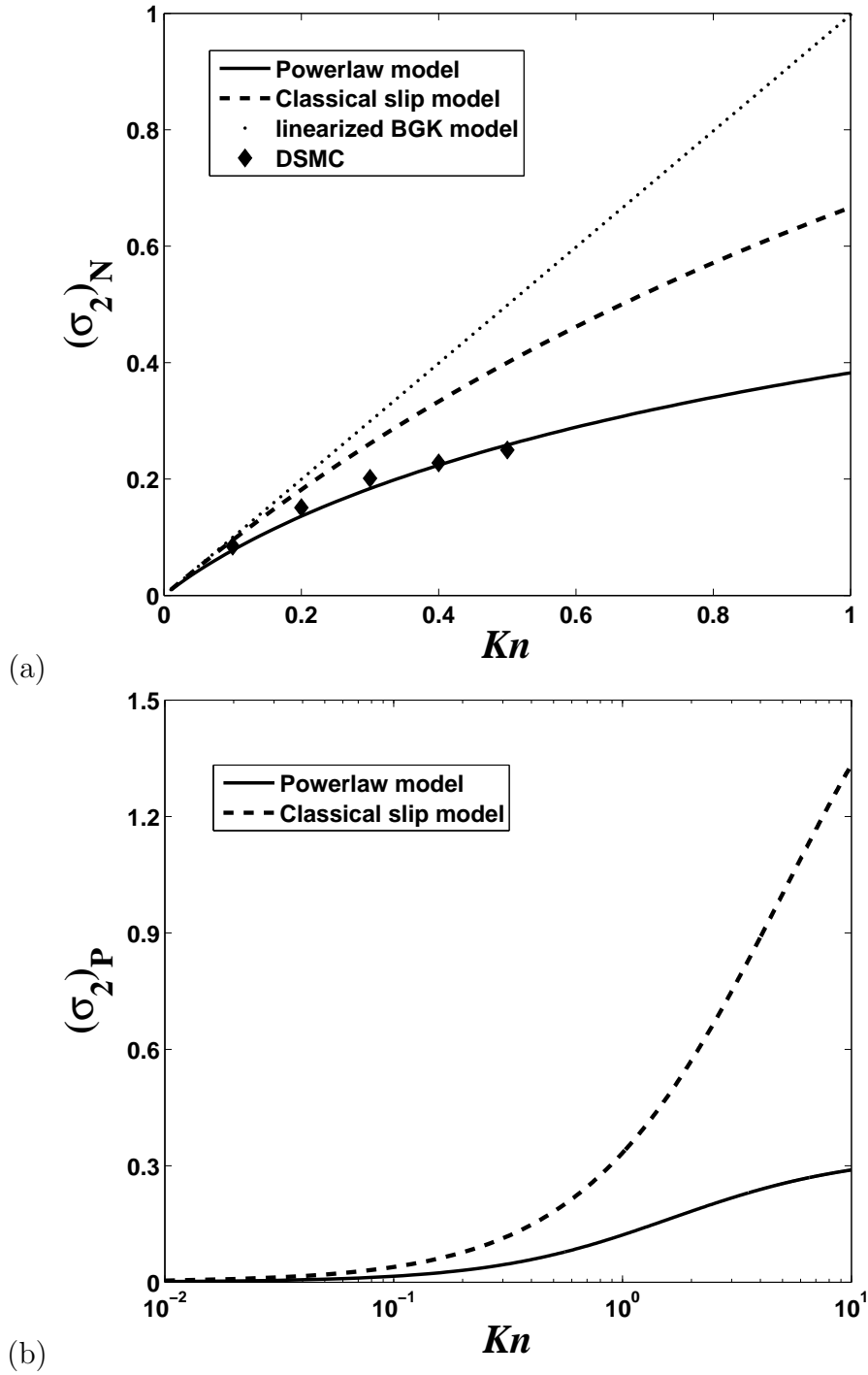
(a)

(b)

Figure 9: Variation of critical accommodation coefficients with Knudsen number for the geometric configuration of $R_2/R_1 = 5/3$; (a) $(\sigma_2)_N$ the lower bound for no velocity inversion, i.e. negative velocity gradient throughout the annular clearance ($R_1 < r < R_2$); (b) $(\sigma_2)_P$ the upper bound for full velocity inversion, i.e. positive velocity gradient throughout the annular clearance.

The gas velocity profiles show good agreement with DSMC data in the transition regime for various values of the accommodation coefficients of the inner and outer cylinder surfaces. When the accommodation coefficients of the inner and outer cylinders have the same value, the family of velocity profiles all pass through a common point. This intersection point for our PL model is very close to the point predicted by the DSMC data, whereas the classical slip solution predicts this point much closer to the outer cylinder. New analytical expressions have been developed for the critical accommodation coefficients for non-inverted, fully inverted and partially inverted velocity profiles. The PL model shows excellent agreement with the available DSMC data.

Our new PL model is more accurate than conventional slip solutions in capturing some of the non-linear effects associated with Knudsen layers in the slip and transition flow regimes. With the current approach, we can also obtain the velocity profile at a fixed Knudsen number by modifying the power-law exponent to provide accurate results in both the Knudsen layer and the bulk flow. Conversely, conventional slip-modeling techniques are only able to modify the velocity-slip at the surface by tuning the value of the slip coefficient.

Our PL mean free path scaling can be readily extended to more complex geometries, and straightforwardly incorporated into existing CFD codes, to solve for low-speed rarefied gas flows in arbitrary geometries. While all our comparisons with DSMC data in the current paper used the PL exponent $n = 3$, as in the previous planar test cases (Dongari et al. 2011a; Dongari et al. 2011b), establishing properly and generally the value of n requires further numerical experiments on rarefied gases confined in arbitrary geometries and subjected to a range of complex flow conditions. Extension to non-isothermal flows should also be the subject of future work.

Acknowledgments

References

Agrawal A, Prabhu SV (2008a) Survey on measurement of tangential momentum accommadation coefficient. J Vacuum Science and Technology A 26: 634-645

Agrawal A, Prabhu SV (2008b) Deduction of slip coefficient in slip and transition regimes from existing cylindrical Couette flow data. Experimental Thermal and Fluid Science 32: 991-996

Aoki K, Yoshida H, Nakanishi T, Garcia AL (2003) Inverted velocity profile in the cylindrical Couette flow of a rarefied gas. Phys Rev E 68 016302

Bahukudumbi P, Park JH, Beskok A (2003) A unified engineering model for steady and unsteady shear-driven gas microflows. Microscale Thermophys Eng 7, 291

Barber RW, Emerson DR (2006) Challenges in modeling gas-phase flow in microchannels: from slip to transition. Heat Transfer Engineering 27(4): 3-12

Barber RW, Sun Y, Gu XJ, Emerson DR (2004) Isothermal slip flow over curved surfaces. Vacuum 76: 73-81.

Beskok A (2001) Validation of a new velocity-slip model for separated gas microflows. Numerical Heat Transfer Part B: Fundamentals 40(6): 451-471

Bird GA (1994) Molecular gas dynamics and the direct simulation of gas flows. Oxford University Press, New York

Burnett D (1935) The distribution of molecular velocities and the mean motion in a non-unifrom gas. Proc. Lond. Math. Soc. 40 382

Cercignani C (1988) The Boltzmann equation and its applications. Springer-Verlag, New York

Chapman S, Cowling TG (1970) Mathematical theory of non-uniform gases. 3rd edition, Cambridge University press

Dongari N, Sharma A, Durst F (2009) Pressure-driven diffusive gas flows in micro-channels: from the Knudsen to the continuum regimes. Microfluidics and nanofluidics 6 (5): 679-692

Dongari N, Durst F, Chakraborty S (2010) Predicting microscale gas flows and rarefaction effects through extended NavierStokesFourier equations from phoretic transport considerations. Microfluidics and nanofluidics 9 (4): 831-846

Dongari N, Zhang YH, Reese JM (2011a) Molecular free path distribution in rarefied gases. J Phys D Appl Phys 44 125502

Dongari N, Zhang YH, Reese JM (2011b) Modeling of Knudsen layer effects in micro/nanoscale gas flows. J Fluid Engg 133(7) 071101

Dongari N, Zhang YH, Reese JM (2011c) Behaviour of microscale gas flows based on a power-law free path distribution function. AIP Conference Proceedings: 1333 724-729

Einzel D, Panzer P, Liu M (1990) Boundary condition for fluid flow: Curved or rough surfaces. Phys Rev Lett 64 2269

Emerson RD, Gu XJ, Stefanov SK, Yuhong S, Barber RW (2007) Nonplanar oscillatory shear flow: From the continuum to the free-molecular regime. Phys Fluids 19 107105

Guest PG (1961) The solid angle subtended by a cylinder. Rev Sci Instrum 32 164

Guo ZL, Shi BC, Zheng CG (2011) Velocity inversion of micro cylindrical Couette flow: A lattice Boltzmann study. Comput Math Appl 61: 3519-3527

Grad H (1949) Note on N-dimensional hermite polynomials. Communications on Pure and Applied Mathematics 2: 325-330

Kennard E H (1938) Kinetic theory of gases with an introduction to statistical mechanics. McGraw-Hill, New York

Kim S (2009) Slip velocity and velocity inversion in a cylindrical Couette flow. Phys Rev E 79 036312

Lilley CR, Sader JE (2007) Velocity gradient singulary and structure of the velocity profile in the Knudsen layer according to the Boltzmann equation. Phys Rev E 76 026315

Lockerby DA, Reese JM, Emerson DR, Barber RW (2004) Velocity boundary condition at solid walls in rarefied gas calculations. Phys Rev E 70 017303

Lockerby DA, Reese JM, Gallis MA (2005) The usefulness of higher-order constitutive relations for describing the Knudsen layer. Phys Fluids 19 100609

Lockerby DA, Reese JM (2008) On the modelling of isothermal gas flows at the microscale. J Fluid Mech 604: 235-261

Maxwell JC (1879) On stresses in rarefied gases arising from inequalities of temperature. Philos Trans R Soc 1 170 231-256

Montroll EW, Scher H (1973) Random walks on lattices. IV. Continuous-time walks and influence of absorbing boundaries. J Stat Phys 9 (2): 101-135

Myong RS, Reese JM, Barber RW, Emerson DR (2005) Velocity slip in microscale cylindrical Couette flow: The Langmuir model. Phys Fluids 17 087105

Schlichting H (1979) Boundary-layer theory. 7th ed. McGraw-Hill, New York

Sone Y (2002) Kinetic theory and fluid dynamics. Birkhauser, Boston

Stefanov SK, Gospodinov P, Cercignani C (1998) Monte Carlo simulation and Navier-Stokes finite difference calculation of unsteady-state rarefied gas flows. Phys Fluids 10 289.

Stefanov SK, Barber RW, Emerson DR, Reese JM (2006) The critical accommodation coefficient for velocity inversion in rarefied cylindrical Couette flow in the slip and near free-molecular regimes. Proc 25th Int Symp on Rarefied Gas Dynamics, St. Petersburg, Russia, edited by M. S. Ivanov and A. K. Rebrov (Publishing House of the Siberian Branch of the Russian Academy of Sciences, Novosibirsk, Russia), pp. 11461151

Stops DW (1970) The mean free path of gas molecules in the transition regime. J Phys D Appl Phys 3 685-696

Tibbs KW, Baras F, Garcia AL (1997) Anomalous flow profile due to the curvature effect on slip length. Phys Rev E 56 2282

Veijola T, Kuisma H, Lahdenpura J, Ryhanen T (1995) Equivalent-circuit model of the squeezed gas film in a silicon accelerometer. Sensors and Actuators A 48: 239-248

Yuhong S, Barber RW, Emerson DR (2005) Inverted velocity profiles in rarefied cylindrical Couette gas flow and the impact of the accommodation coefficient. Phys Fluids 17 047102

Zhang YH, Gu XJ, Barber RW, Emerson DR (2006) Capturing Knudsen layer phenomena using a lattice Boltzmann model. Phys Rev E 74 046704